Ring formation and the structural and electronic properties of tetrahedral amorphous carbon surfaces

Jianjun Dong and David A. Drabold

Department of Physics and Astronomy, Condensed Matter and Surface Science Program, Ohio University, Athens, Ohio 45701-2979

In this paper, we report first-principles structural models of surfaces of tetrahedral amorphous carbon (ta-C). The topology and defect structure of the amorphous surfaces are analyzed at the atomistic level. We examine the transition of the local bonding environment from the bulk to the surface. Comparing the surface with the bulk, many more surface atoms are threefold coordinated and planar rings or chains are formed with the sp^2 bonds. This ''graphization'' character of the ta-C surface also significantly influences its electronic properties. Electrons are easily delocalized within these surface sp^2 rings/chains and some of the surface electronic eigenstates become extended along the surface through such rings/chains. The implications of surface graphization for the growth and surface conduction are briefly discussed. [S0163-1829(98)03724-2]

I. INTRODUCTION

From an applied point of view, the tetrahedral amorphous carbon (ta-C) thin film is a very promising electronic material.[1–3] Depite its disordered structure, ta-C still possesses a very high fraction of sp^3 content (up to 90%, depending on the deposition process[4,5]) and is a wide-band-gap ($E_g=2$ eV) semiconductor.[6] Much research has been done to study its doping and transport properties.[6–10] Recently, several researchers also began to explore substituting polycrystalline diamond with a ta-C thin film in low-field electron emission imaging.[11–13]

Since McKenzie and co-workers successfully demonstrated the deposition of a high-quality ta-C thin film using a filtered cathodic arc in 1991,[4] extensive experimental and theoretical work has been devoted to understand the fundamental properties of ta-C. In theoretical work, several groups have presented structural models of *bulk ta-C* based on different computational methods ranging from empirical potential to first-principles electronic structure based techniques.[10,14–21] Several growth models were also proposed.[3,22] Yet, the growing mechanism is still not fully understood. There are still extensive discussions in experimental works about the growth mechanisms of ta-C thin films.[23–26] In this paper, we report our recent study of a model *surface* structure of ta-C thin films. Understanding properties of the *static, equilibrium* structure of surface is an essential precursor to understanding growth.

Correctly modeling the disordered structure of amorphous solids is always a challenge for computational solid state physics. The task is further complicated on amorphous surfaces. For ta-C surfaces, at least to our knowledge, there is no definite experimental measurement of the surface sp^3 concentration, although it is widely believed and qualitatively observed that the surface has more sp^2 graphitelike characteristics than its bulk.[27] The meager *a priori* information about the atomic structure and the rich complexity of local bonding on the amorphous surfaces limits the suitability of various empirical techniques whose validity usually depends on the assumption that the system to be studied is close to those systems where the adjustable parameters are fitted.[28] Therefore, first-principles techniques, which have no

fitting parameters and are transferable in various local bonding environment, are needed to correctly describe the structure of ta-C surfaces. In this paper, we present our study of ta-C surfaces using an approximate first-principles, local orbital electronic structure based technique.

It is known that no first-principles structural models are able to directly represent the typical surfaces in the real thin film growth because the time scale of the numerical molecular dynamical simulations is too short compared to experiments. However, they do reveal the possible defect types that are likely on the ta-C surfaces and the intrinsic relation between the electronic defects and the corresponding bonding geometry of atoms. Because of computational limitations, we have to use supercells with artificial periodic boundary conditions (along the x and y directions) to model the infinite slabs. Although our supercell models are among the largest of this kind of calculation, finite size artifacts still influence our calculations. We will discuss this point later in detail.

In our study, we use a first-principles quantum molecular dynamics technique to model and analyze the microstructure of the ta-C surface. We find that there is significant local bonding reconstruction on the surface layers and surface geometrical defects induce some surface states in the electronic band tails. Some surface states are tightly localized, while some are extended along the surface through sp^2 rings or chains.

II. COMPUTATIONAL METHODOLOGY

In this paper, all the calculations are based on first-principles, local orbital electronic structure methods developed by Sankey and Niklewski. Details of this technique were given in their original paper[29] and elsewhere.[30] Briefly speaking, this method is theoretically founded on the density functional theory within the local density approximation (LDA) and the nonlocal pseudopotential scheme. Two important characteristics of this scheme are (i) instead of using plane waves to expand the one electron eigenstates, a set of four compact pseudoatomic orbitals (within a confinement radius of $r_C=4.1a_B$ for carbon) per atom site is used as *local*

basis and (ii) the total energy is approximated in the non-self-consistent Harris functional, which is a stationary principle suitable for the systems where charge transfer is not large. The local basis and Harris functional make this scheme more efficient to study larger systems. This advantage is more significant in the calculations of microclusters and surfaces, where periodic boundary conditions (at least in one of three directions) are not applied. The suitability of this local orbital, Harris functional LDA method to describe carbon structures in a very wide range of bonding environment was proved by the computation of the phase diagram[28] and further extensive studies of carbon microclusters,[31] fullerenes,[32] ta-C bulk,[19,10] and diamond surfaces[33,34] have been performed with this method and the results are close to those of self-consistent plane wave calculations and experimental results (if available).[35,36,20]

Using the same LDA molecular techniques described above, Stumm, Drabold, and Fedders proposed a 216-atom bulk ta-C model[10] by relaxing a rescaled amorphous diamond model provided by Djordjevic, Thorpe, and Wooten.[17] Amorphous diamond is an artificial solid that is related to ta-C. The initial amorphous-diamond model is at the crystalline diamond density (3.5 g/cm^3) and is entirely fourfold-coordinated. After the rescaling and LDA relaxation, the bulk model is at the experimental ta-C density (3.0 g/cm^3) and has high fraction of sp^3 content (88%). Among those sp^2 bonded atoms, 90% form π bonded pairs (or triplets). The highest occupied molecular orbital to lowest unoccupied molecular orbital gap is 1.08 eV in this supercell model and the π-π^* gap is 1.26 eV. The calculated electronic properties are consistent with optical experiments.[6] Readers can refer to previous publications for details.[19,10] To model the surface we first break the periodic continuation along the z direction to transform the periodically extended cube into an infinite slab with two free surfaces (one labeled as the "top" surface and the other as the "bottom" surface). Then the slab is relaxed through our LDA molecular dynamics simulation to search for the new minimal energy configuration under the surface condition. With a time step $\Delta t = 0.5$ fs, the slab was heated briefly (0.2 ps) to a high temperature, annealed at 300 K for about 0.8 ps, and finally quenched to 0 K. Two models were made using the above procedures with the only difference being in at high temperature for the first step: 2000 K for the first model (called slab model I) and 6000 K for the second model (called slab model II). When the models are heated to high temperatures, some atoms may escape surfaces. So we remove such isolated atoms from our slab models and finally slab model I contains 213 atoms per supercell and slab model II contains 210 atoms per supercell.

III. SURFACE STRUCTURE

After the periodic boundary condition along the z axis is broken, dangling bonds will appear on the surfaces. Thorough structural relaxation will lead to some major local bonding rearrangements (the amorphous analog of crystalline surface reconstruction) near the surfaces. The total energies of slab model I and slab model II are about 0.25 eV/atom and 0.11 eV/atom lower than the unreconstructed ta-C surface model respectively.[37] As the total energy of the structure is one (incomplete) measure of the credibility of amor-
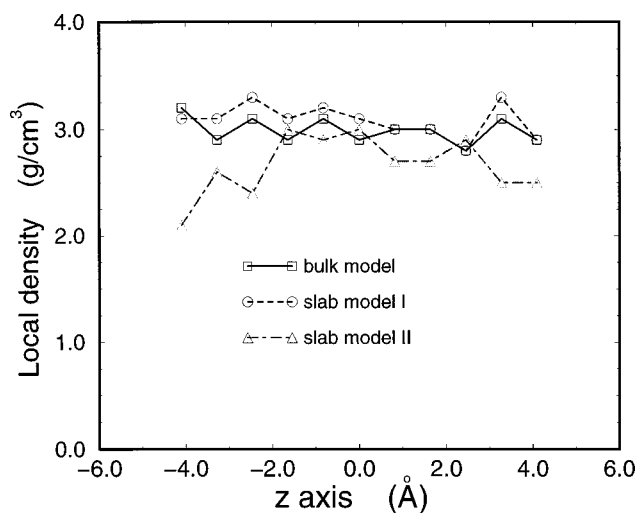

FIG. 1. Local density (averaged over a 3 Å thickness) at different depths of bulk and surface models of ta-C.

phous models, we think that slab model I is more energetically stable and therefore we will concentrate on it. Slab model II has a little higher total energy, but there is still structural reconstruction on the surfaces. So we also discuss this model sometimes for comparison.

Initially at the bulk density (3.0 g/cm^2), our slab models expand slightly along the normal direction of the surface during relaxation. In Fig. 1, we show the local density (averaged in the neighborhood of 3 Å) at different depths of the bulk models and the two slab models we created. Slab model I (the one that was heated at 2000 K) is almost as homogeneous as the bulk phase with only a small local density fluctuation, while slab model II (the one heated at 6000 K) shows a significant decrease of the local density around surface region. Although our numerical modeling process does not correspond to the *natural* process, our result suggests that kinetic energy of carbon atoms (or ions) is an important parameter in growth: Too much kinetic energy may cause carbon atoms to condense at lower densities. This perhaps relates to the bombardment-induced damage observed in the growth.[23,26] Figure 1 further suggests that slab model I corresponds to a high-quality ta-C surface and slab model II may be related to the surface of some form of low-quality ta-C thin film.

To focus on the surface character of our slab models, we choose the 50 atoms closest to vacuum above (or below) as the top (or bottom) surface. This definition of surface is of course arbitrary, but it reasonably reflects the top two surface layers. The surface projected pair distribution function $g(r)$ is shown in Fig. 2. Similarly to the bulk phase, the surface $g(r)$ shows a first peak at 1.54 Å, which is the bond length in diamond, and a second peak around 2.54 Å, which is the distance between the second nearest neighbors of the tetrahedral bond angle. More interestingly, in the $g(r)$ of slab model I, there appear two small peaks on the right-hand side of the first and second peaks, which we label by arrows 1 and 2 in the plot. The first small peak appears around 1.34 Å, which is the bond length in graphite. This strongly suggests that although sp^3 hybridization is still dominant, the sp^2 content on the surfaces increases significantly. The second small peak near 2.25 Å could be the distance between the
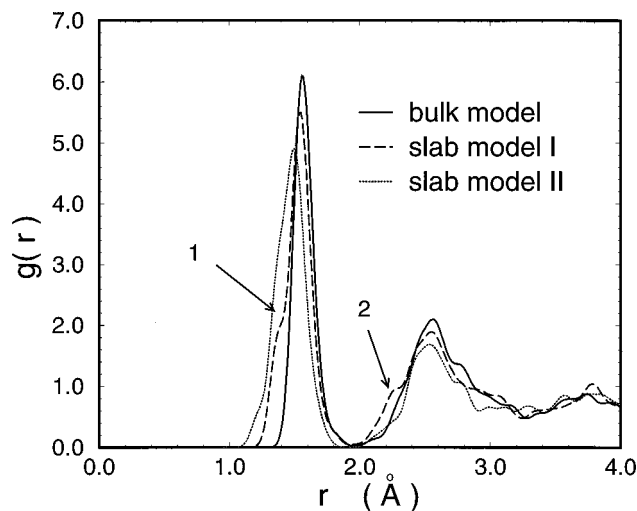
FIG. 2. Pair distribution function $g(r)$. The data of slab models are surface projected.

FIG. 3. Local fraction of each type of coordination (averaged over a 1 Å thickness) through the whole slab model I.

second nearest neighbors if the bond angle decreases to 90°. We find that such a large angle distortion can be found in fourfold rings and believe that the increasing occurrence of fourfold rings around surface layers causes the second small peak near the major second peak in the surface projected $g(r)$. We predict that this feature will be observed if surface sensitive diffraction measurements are performed. The increase of fourfold rings will be discussed in detail in the following. $g(r)$ of slab model II shows an obvious shifting of first peak, which indicates that the less-dense, low-quality amorphous carbon surface has more sp^2 and sp^1 content.

The statistics of the number of atoms of each type of coordination is listed in Table I.[38] Approximately, we can regard the fourfold-coordinated atoms in the models as the sp^3 content observed in experiments. We notice that 72% of the non-fourfold-coordinated atoms are within the top or bottom surface layers and the fraction of fourfold-coordinated atoms drops dramatically from 88% in the bulk to about 46% on the surfaces. The variation of sp^3 and sp^2 content with the depth of our slab model I is indicated in Fig. 3. We find that twofold-coordinated sites only appear in the top or bottom layers. The local fraction of fourfold-coordinated sites peaks in the middle of the slab (as high as 90%) and drops when approaching either the top or bottom layers (only about 20% in the outermost layers). At the same time, the fraction of threefold-coordinated sites increases from around 20% in the middle of the slab to more than 60% in the outermost layers. Our finding here is consistent with the experiments,
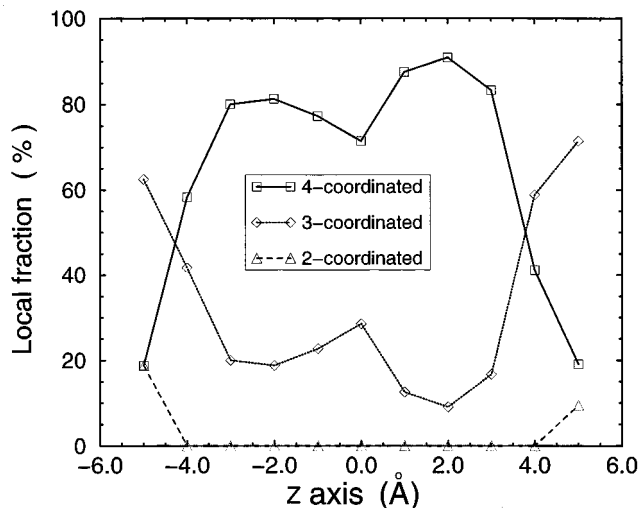
which observe much more sp^2 content on the ta-C surfaces.[27]

The microstructure of the surface layers (top 50 atoms or bottom 50 atoms) of slab model I is clearly shown in Fig. 4. Threefold-coordinated atoms are emphasized with a darker gray scale and twofold-coordinated atoms are represented by white circles. As in the bulk, threefold-coordinated atoms tend not to be isolated. Only 2 out of 49 of them have dangling bonds. Since many of them segregate at the surface region, they usually connect into chains or closed planar rings. The bond length between these threefold-coordinated atoms reflects the C=C double π bond character. We find a sevenfold ring that consists of only threefold-coordinated atoms at the top of our slab model and a sixfold ring that consists of five threefold atoms and one fourfold atom at the bottom. This shows the tendency of ''graphization'' at ta-C surfaces. We think that the reason that no exact sp^2 bonded planar graphite ring appears in this particular model is only because of the limitation of the finite size of this cell. Indeed, in a related study of the amorphous-diamond surface, we observed such exact graphite rings.[39] The ringed or chained threefold-coordinated carbon atoms make the surface topology less diamondlike and more graphitelike than its bulk. This ring/chain forming structure is the major difference between the ta-C surface and a-Si surface. Unlike carbon atoms that are more ''flexible'' about the sp, sp^2, or sp^3 bonding, silicon atoms have a much stronger propensity for bonding at the tetrahedral angle. Consequently, many iso-

TABLE I. Coordination of C atoms in the ta-C model for surface I.

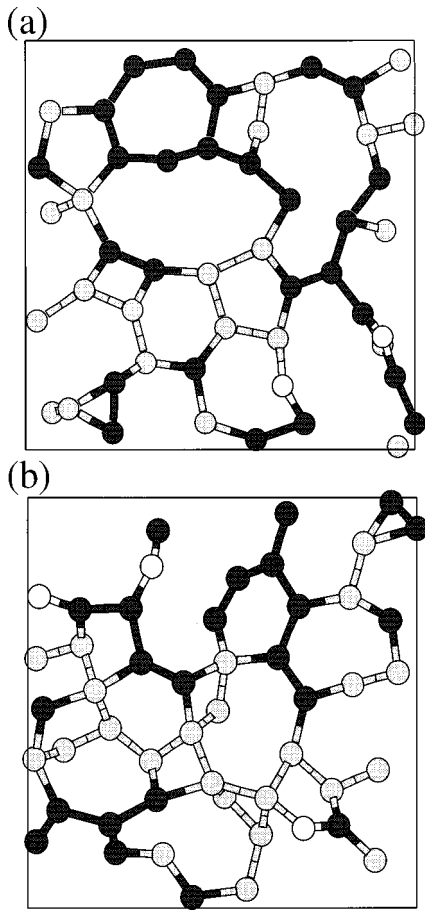|	No. of neighbors	No. of atoms	Percentage
Whole slab (213 atoms)	2	5	3%
	3	70	33%
	4	138	64%
Surface only (100 atoms)	2	5	5%
	3	49	49%
	4	46	46%

FIG. 4. The 2D top (or bottom) view of the surface layers of slab model I. The periodic boundary conditions are imposed in the plane of the figure. The gray scale in this figure represents the types of coordination of each atom: light, fourfold-coordinated atom; dark, threefold-coordinated atom; white, twofold-coordinated atom.

FIG. 5. The 2D top (or bottom) view of the surface layers of slab model II. See the caption of Fig. 4.

lated dangling bonds (instead of sp^2 bonded) form on the a-Si surface.[40]

Although graphization is significant on the ta-C surface, about 50% of the atoms still remain fourfold coordinated. To fit into relatively planar surfaces, bond angles between these fourfold-coordinated atoms are sometimes quite different from the tetrahedral angle. Indeed, we find six fourfold rings. Some fourfold rings also contain the twofold-coordinated atoms with two dangling bonds emerging from the surface layers. The bond angles in the fourfold rings are usually around 90°. Fourfold rings are rare in the bulk phase of amorphous tetrahedral solids because of the large bond angle distortion involved. However, on the ta-C surfaces, fourfold
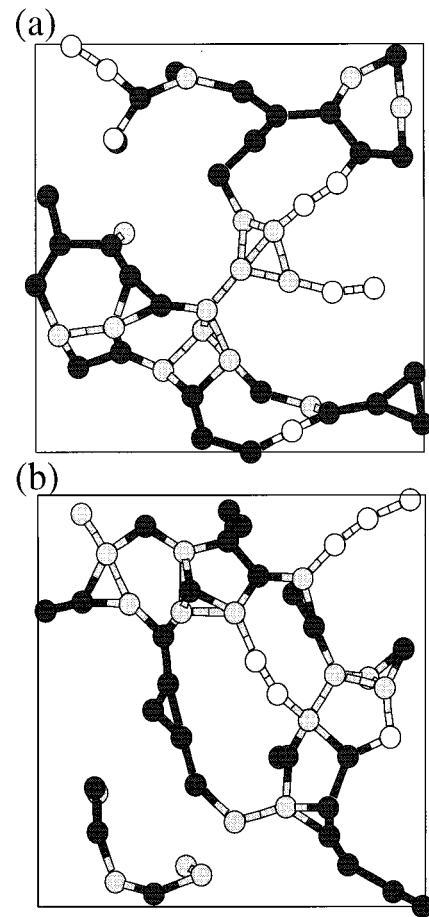
rings may occur with a higher probability with the energy compensated for by avoiding bond stretching.

Our second surface model is also analyzed (Table II) and pictured in Fig. 5. We find that the fraction of fourfold-coordinated atoms on the surfaces dramatically reduced to about 30%. Although more threefold and twofold atoms appear, they do not form a very regular ring pattern within the first two surface layers. This indicates that the surface layers of slab model II are less planar. From a side view, we observe that they are a little rougher than those of slab model I. This observation is consistent with the earlier experimental measurement by Park *et al.*[25] They found that among the films grown under different conditions, those with higher sp^2 contents are rougher.

Due to the difference in the local bonding, graphitelike

TABLE II. Coordination of C atoms in another model for surface II.

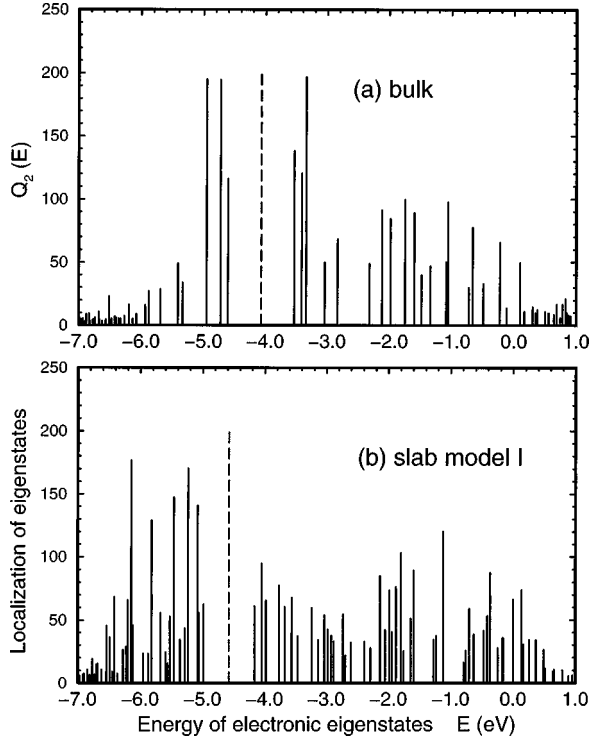|	No. of neighbors	No. of atoms	Percentage
Whole slab (210 atoms)	2	17	8%
	3	89	42%
	4	104	50%
Surface only (100 atoms)	2	14	14%
	3	54	54%
	4	32	32%

FIG. 6. Electronic eigenstates in the band gap region for the (a) bulk model and (b) slab model I. The positions of solid vertical bars represent the eigenvalues of electronic eigenstates and the height of the bars is the spatial localization $Q_2(E)$ (see the text). The Fermi levels are indicated by the long dashed lines in the figure.

sites, diamondlike sites, and dangling bond sites are quite different in their chemical reactivity, which will greatly influence the tendency in the thin film growth processes. A quantitative conclusion could be drawn if further calculations of single adatom binding energies at different surface sites are performed.[41] Such binding energy data could be used in some empirical Monte Carlo growth simulation techniques.

IV. ELECTRONIC PROPERTIES

Bonding topology usually manifests itself in electronic properties. Since our previous structural analysis shows that slab model II is less relevant to the surface of high-quality ta-C thin films, here we discuss only slab model I. Figure 6 shows the individual electronic eigenstates near the band gap. For the convenience of comparison, the eigenstates of bulk ta-C (Ref. 10) are shown in the top panel and the eigenstates of surface ta-C thin films are shown in the bottom panel. These states are usually referred to as midgap or band tail states and are obviously important to transport, optical, and doping properties of solids because of their proximity to the Fermi level (located by the long vertical dashed line in the figure). In this figure, each vertical bar locates the position of an eigenstate and its height is the eigenstate's spatial charge localization quantified by $Q_2(E)$:

$$Q_2(E) = N \sum_{n=1}^{N} q(n,E)^2. \qquad (1)$$

Here N is the number of atoms in the slab model and $q(n,E)$ is the Mulliken charge[42] localized on atom site n in a certain

eigenstates E. $Q_2(E)$ has a minimal value of 1 if an eigenstate E is uniform among all the atom sites and has a maximal value of N if the charge of an eigenstate E is localized only at one atom site. Larger $Q_2(E)$ means that the eigenstate is more localized in real space.

To examine the atomistic spatial structure of an electronic eigenstate, we try to ''visualize'' the states as follows. (i) For a given electronic eigenstate, the electron charge associated with each atom site is computed. (ii) Then each atom is drawn in one of the four levels of the gray scale according to the amount of charge associated with it. Black atoms are strong localization sites that contribute more than 10% of total charge each, less dark atoms are sites that contribute more than 2.5%, light atoms are sites that contribute more than 1% each, and white atoms contribute the rest. For clarity, only 90% of the total charge is present and those atoms that contribute the least charge for the given eigenstate are omitted in the figure.

Previous studies on bulk ta-C show that *strongly* localized states in the midgap or at the top of the band tail [for example, the three top valence states in Fig. 6(a)] are induced by the bulk defects.[19,10] If we examine every state from the Fermi level down to the inside valence states, we will find that the spatial character of these eigenstates goes through a so-called Anderson (localized-to-extended) transition. The nature of the Anderson transition due to the topological disorder is very important to transport and doping. We recently reported a study of the Anderson transition of electronic band tail states in tetrahedral amorphous semiconductors based on a 4096-atom a-Si model.[43]

In our ta-C surface slab model, there are obviously more states right below the Fermi level (within the 1.5-eV range). Many of these states have *surface* character. We find that the extended-to-localized transition of electronic eigenstates proceeds from the ''bulk-to-surface'' transition on the ta-C surface. In the surface slab model, the states from inside the valence band [Fig. 7(a)] are still bulklike extended states. From these states, we do not observe any significant charge localization caused by any surface atoms. When we consider the energy range from -7.0 to -6.5 eV, states [Fig. 7(b)] are still quite extended; yet, the influence from surface atoms increases. The influence from surface atoms becomes dominant when the energy approaches -6.4 eV [Fig. 7(c)]. In some extremely localized *surface* states [Fig. 7(d)], up to 80% of the total charge in such a state is localized at the top surface.

The five strongly localized surface valence states [$Q_2(E)$ values larger than 100] are found to be caused by severe *surface* structural defects, including dangling bonds from twofold atoms and/or fourfold rings. It is expected that such severely distorted and uncommon surface defects can induce tightly localized electronic eigenstates. One of these five states is shown in Fig. 8(a). Referring to the structural model of the bottom surface shown in Fig. 4(b), we can easily identify that the three twofold atoms located in lower-right or upper-left corners of the bottom surface layer are among the strongest localization atom sites.

The most interesting electronic features of the ta-C surface are among those less-localized surface states, which are also the majority of states slightly below the Fermi level. These surface states are localized among the common

(a) E= -10.920 eV, Q_2 (E)= 2.7   (c) E= -6.416 eV, Q_2 (E)= 68.4

(b) E= -6.811 eV, Q_2 (E)= 6.9   (d) E= -5.283 eV, Q_2 (E)= 43.7
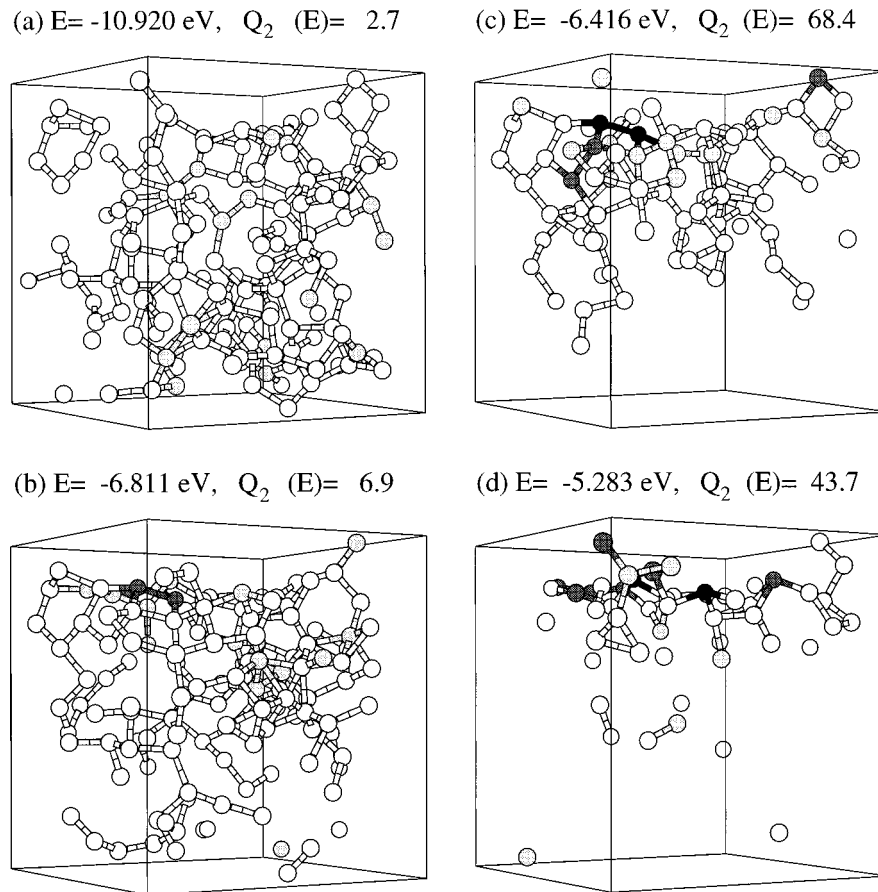
FIG. 7. Spatial character of the bulk-to-surface transition of valence electronic states in the surface slab model I. For a given eigenstate [its energy eigenvalue and Q_2 value (see the text) are shown at the top of each supercell], the electron charge density is depicted according to the four-level gray scale. Each atom is shown according to the fraction of total charge: very dark ($\geq$10%), less dark ($\geq$2.5%), light ($\geq$1.0%), white ($\leq$1.0%), such that at least 90% of the total charge is shown. The electronic states evolve from (a) a bulklike extended state in the middle of the valence band to (b) a less extended state, to (c) a more surfacelike state, to (d) a surfacelike localized state.

threefold-coordinated surface defects. Due to the sp^2 ring/chain formation discussed earlier in this paper, electrons in such surface states are easily delocalized among these rings or chains. Figure 8(b) shows a typical surface state of this kind. Referring to the structural model of the top surface in Fig. 4(a), this eigenstate clearly extends over the two connected rings that are mostly made of the threefold-coordinated atoms. In some other cases, we also find that some surface states extend along the threefold-coordinated chains. The delocalization of surface states through sp^2 rings/chains is also related to the resonant cluster proliferation model we proposed in our recent study of the Anderson transition in the band tail states of a-Si.[43] The ''simple physics'' here is just the *resonant tunneling* between clusters (such as sp^2 rings) with similar electronic energies. It is plausible that electrons in such delocalized surface states may be conducted along the surface through these graphitized rings/chains formed on the ta-C surface. A microscopic calculation of the surface electrical conductivity will be performed based on the information of these electron eigenstates and we will report the result elsewhere.

Because the electronic energy range of surface states overlaps with those bulk defect states, they will interact with each other if they are also spatially close. In this current slab model, we do not find any electronic eigenstates solely localized in the bulk. We think that this is an artifact of the small supercell model. In our model, we find that some defects in the middle of the supercell do interact with the surface defects. We believe that such an interaction is akin to the interaction of surface defects and subsurface defects in the real ta-C thin film. Such states usually consist of two or more localization centers, some located in the surface layers and some located in the middle of the supercell. Two such states are shown in Fig. 9. It is hard to have tightly localized states in the subsurface layers in ta-C because such states are usually influenced by the surface defects. Such defect interactions can make an eigenstate extend from surface layers into subsurface layers. However, obviously, delocalization through such a defect interaction mechanism has a lesser possibility in the thicker supercell model. Similar defect interactions were also observed in the previous study of the surface of a-Si.[40]

We find that the character of the conduction states in our surface model is similar to that of the valence states. The only difference we find is that defects and surface conduction states mostly lie within the large pseudo-band-gap region instead of small-band-tail region. The top four conduction states have more charge localized in the middle than on the surface layers, which means that the interaction between subsurface defects and surface defects is not as strong as in valence states. Part of the reason is that the energy range of the surface states does not totally overlap with the bulk de-
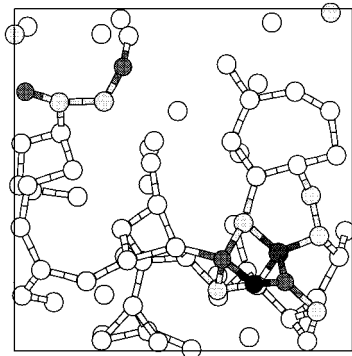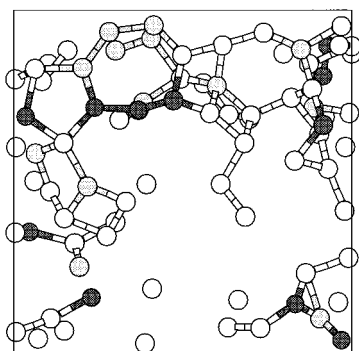
(a) E= -6.144 eV, Q_2 (E)= 176.6

(a) E= -5.360 eV, Q_2 (E)= 34.3

(b) E= -5.561 eV, Q_2 (E)= 15.8

(b) E= -5.053 eV, Q_2 (E)= 55.6

FIG. 8. Two different types of *surface* electronic eigenstates: (a) a tightly localized surface state confined around twofold defect atoms at the bottom surface layers and (b) a less localized surface state delocalized within two sp^2 rings at the top surface layers. The gray scales represent the charge localization (see the caption of Fig. 7). The microstructure of the bottom and top surface layers are also shown in Figs. 6(b) and 6(a), respectively. The periodic boundary conditions are imposed in the plane of the figure.

FIG. 9. Spatial character of two valence defect states. Due to the interaction of surface structural defects and subsurface structural defects, the defect states penetrate from surface layers into subsurface layers. See the caption of Fig. 7 for the interpretation of gray scales.

fects in the pseudo-band-gap region and therefore it is possible that the subsurface defects are more energetically distant from surface defects.

V. CONCLUSIONS

In this study, we reported a structural model of *ta*-C surfaces constructed with first-principles molecular dynamics techniques. Our model surfaces are consistent with the experimental observations that high-quality *ta*-C thin films have atomically smooth surfaces and a high graphitelike sp^2 content. The fraction of sp^3 atoms on the surfaces seems to be near 50%. We find that a major feature of *ta*-C surfaces is that threefold-coordinated atoms tend to congregate into
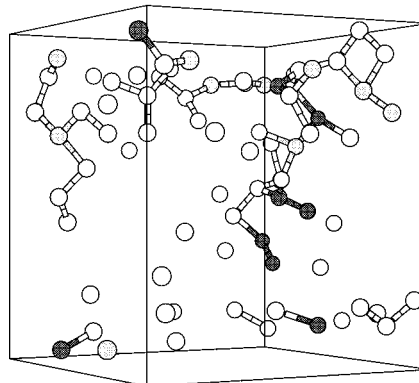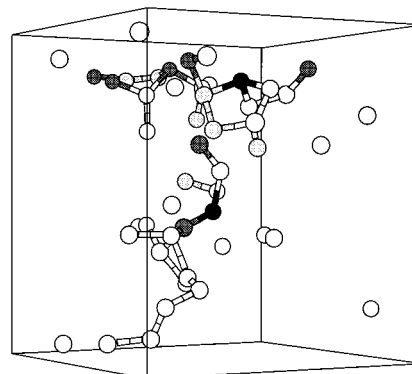
chains or rings to cause ''surface graphization.'' With regard to electronic states, we observe the states evolve from bulk-like extended states inside the bands to surfacelike localized states in the band tail or band gap. Although severe surface defects can induce tightly localized surface electronic eigenstates, surface sp^2 graphization also delocalizes the surface states along the surface. Further investigations on the surface binding energies and surface conductivity will be done and reported elsewhere.

[1] D. R. McKenzie, D. A. Muller, B. A. Pailthorpe, Z. H. Wang, E. Kravtchinskaia, D. Segal, P. B. Lukins, P. D. Swift, P. J. Martin, G. A. J. Amaratunga, P. H. Gaskell, and A. Saeed, Diamond Relat. Mater. **1**, 51 (1991).

[2] J. Robertson, Surf. Coat. Technol. **50**, 185 (1992).

[3] D. R. McKenzie, Y. Yin, N. A. Marks, C. A. Davis, E. Kravtch-inskaia, B. A. Pailthorpe, and G. A. J. Amaratunga, J. Non-Cryst. Solids **164-166**, 1101 (1993).

[4] D. R. McKenzie, D. A. Muller, and B. A. Pailthorpe, Phys. Rev. Lett. **67**, 773 (1991).

[5] P. H. Gaskell, A. Saeed, P. Chieux, and D. R. McKenzie, Phys. Rev. Lett. **67**, 1286 (1991).

[6] V. S. Veerasamy, G. A. J. Amaratunga, C. A. Davis, A. E. Timbs, W. I. Milne, and D. R. McKenzie, J. Phys.: Condens. Matter 5, L169 (1993).

[7] V. S. Veerasamy, J. Yuan, G. A. J. Amaratunga, W. I. Milne, K. W. R. Gilkes, M. Weiler, and L. M. Brown, Phys. Rev. B 48, 17 954 (1993).

[8] C. Ronning, U. Griesmeier, M. Gross, H. C. Hofsaess, R. G. Downing, and G. P. Lamaze, Diamond Relat. Mater. 4, 666 (1995).

[9] J. Robertson and C. A. Davis, Diamond Relat. Mater. 4, 441 (1995).

[10] P. Stumm, D. A. Drabold, and P. A. Fedders, J. Appl. Phys. 81, 1289 (1997).

[11] B. S. Statyanarayana, A. Hart, W. I. Milne, and J. Robertson, Appl. Phys. Lett. 71, 1430 (1997).

[12] K. C. Park, J. H. Moon, S. J. Chung, J. Jang, M. H. Oh, and W. I. Milne, Appl. Phys. Lett. 70, 1381 (1997).

[13] L. S. Pan, T. E. Felter, D. A. Ohlberg, W. L. Hsu, C. A. Fox, R. Cao, and G. Vergara, J. Appl. Phys. 82, 2624 (1997).

[14] J. Tersoff, Phys. Rev. B 44, 12 039 (1991).

[15] P. C. Kelires, C. H. Lee, and W. R. Lambrecht, J. Non-Cryst. Solids 164-166, 1131 (1993); P. C. Kelires, Phys. Rev. Lett. 73, 2460 (1994).

[16] C. Z. Wang and K. M. Ho, Phys. Rev. Lett. 71, 1184 (1993).

[17] B. R. Djordjevic, M. F. Thorpe, and F. Wooten, Phys. Rev. B 52, 5685 (1995).

[18] Th. Frauenheim, P. Blaudeck, U. Stephan, and G. Jungnickel, Phys. Rev. B 48, 4823 (1993); U. Stephan, Th. Frauenheim, P. Blaudeck, and G. Jungnickel, ibid. 50, 1489 (1994).

[19] D. A. Drabold, P. A. Fedders, and P. Stumm, Phys. Rev. B 49, 16 415 (1994).

[20] D. A. Drabold, P. A. Fedders, and M. P. Grumbach, Phys. Rev. B 54, 5480 (1996).

[21] N. A. Marks, D. R. McKenzie, B. A. Pailthorpe, M. Bernasconi, and M. Parrinello, Phys. Rev. Lett. 76, 768 (1996).

[22] J. Robertson, J. Non-Cryst. Solids 164-166, 1115 (1993).

[23] P. J. Fallon, V. S. Veerasamy, C. A. Davis, J. Robertson, G. A. J. Amaratunga, W. I. Milne, and J. Koskinen, Phys. Rev. B 48, 4777 (1993).

[24] F. Qian, R. K. Singh, S. K. Dutta, and P. P. Pronko, Appl. Phys. Lett. 67, 3120 (1995).

[25] H. Park, Y. K. Hong, J. S. Kim, C. Park, and J. K. Kim, Appl. Phys. Lett. 69, 779 (1991).

[26] H. C. Ong and R. P. H. Chang, Phys. Rev. B 55, 13 213 (1997).

[27] C. A. Davis, K. M. Knowles, and G.A. J. Amaratunga, Surf. Coat. Technol. 76-77, 316 (1995).

[28] D. A. Drabold, P. Stumm, and P. A. Fedders, Phys. Rev. Lett. 72, 2666 (1994).

[29] O. F. Sankey and D. J. Niklewski, Phys. Rev. B 40, 3979 (1989).

[30] D. A. Drabold, in Amorphous Insulators and Semiconductors, edited by M. F. Thorpe and M. I. Mitkova (Kluwer, Dordrecht, 1997).

[31] D. A. Drabold, R. Wang, S. Klemm, O. F. Sankey, and J. D. Dow, Phys. Rev. B 43, 5132 (1991).

[32] G. B. Adams, J. B. Page, O. F. Sankey, K. Sinha, J. Menendez, and D. R. Huffman, Phys. Rev. B 44, 4052 (1991); G. B. Adams, O. F. Sankey, J. B. Page, M. O'Keeffe, and D. A. Drabold, Science 256, 1792 (1992).

[33] S. H. Yang, D. A. Drabold, and J. B. Adams, Phys. Rev. B 48, 5261 (1993).

[34] D. R. Alfonso, S. H. Yang, and D. A. Drabold, Phys. Rev. B 50, 15 369 (1994).

[35] S. Fahy and S. G. Louie, Phys. Rev. B 36, 3373 (1987).

[36] G. Galli, R. M. Martin, R. Car, and M. Parrinello, Phys. Rev. B 42, 7470 (1990).

[37] Note that the total energies we describe here are not surface energies. They are summed over all the atoms in the supercell including both surface atoms and atoms in the middle.

[38] In this study, we choose the value of the maximum C-C bond length as $r_{max} = 1.8$ Å to count the number of coordinations. This value is consistent with the position of the first minimal in the pair distribution function $g(r)$. We find that our analysis will not change qualitatively if we use a little larger or smaller values.

[39] J. Dong and D. A. Drabold (unpublished).

[40] K. A. Killan, D. A. Drabold, and J. B. Adams, Phys. Rev. B 48, 17 393 (1993).

[41] J. Wang, D. A. Drabold, and A. Rockett, Appl. Phys. Lett. 66, 1954 (1995).

[42] A. Szabo and N. S. Ostlund, Modern Quantum Chemistry (Dover, New York, 1996).

[43] J. Dong and D. A. Drabold, Phys. Rev. Lett. 80, 1928 (1998).

[44] Remember that the gray scale used in the two figures has different meaning: a different gray scale represents a different number of coordinations in Fig. 4, but shows a different amount of charge localization in Fig. 8. See the captions of the two figures.